Wireless Charging Power Control for HESS through Receiver Side Voltage Control

Toshiyuki Hiramatsu*, Xiaoliang, Huang†, Masaki Kato†, Takehiro Imura†, and Yoichi Hori†
*Department of Electric Engineering
The University of Tokyo
Kashiwanoha, Kashiwa, Chiba, Japan
Email: hiramatsu@hflab.k.u-tokyo.ac.jp
†Graduate School of Frontier Science
The University of Tokyo
Kashiwanoha, Kashiwa, Chiba, Japan

***Abstract*—Battery/Supercapacitor (SC) hybrid energy storage system (HESS) is widely researched due to the superiority of SC in high power density, high cycle capability, and long life time. The repetitive charge for HESS via Wireless Power Transfer (WPT) is a potential solution for reduction of battery size on board. For WPT charging, the load impedance control using DC-DC converter was proposed to improve the transmission efficiency. The charge power control is also necessary because of the limited capacity of HESS. Moreover, the power control should be done on the receiver side to simplify the configuration of transmission side. In this paper, charge power control via WPT without communication between transmitter and receiver side is proposed. The proposed method applied the feedforward controller is verified by experiments.**

I. Introduction

Energy storage systems are significant key in electric vehicles (EVs) and electric operational machines. One of the commonly used energy storage devices is the battery. However, a battery has three critical disadvantages, the first problem is its slow response speed because battery stores energy with chemical reactions. Secondly, the energy density is lower than the combustion engine. Lastly, a battery has a short lifetime because it is damaged by charging and discharging. A conventional solution for these problems is to be equipped with a huge battery on board which increases the cost and heavy weight of the energy storage system.

In order to solve these problems, the Battery/Supercapacitor (SC) Hybrid Energy Storage System (HESS) has been proposed [1][2]. A SC as energy storage device has been widely used in several applications because the SC has a high power density, high cycling capability, and a long life time [3]. Due to these advantages of the SC, HESS for EVs application can achieve high acceleration performance, high efficiency for regenerative braking, extension of battery life, and a low cost.

The energy capacity of HESS is limited and much lower than the combustion engine. In order to improve the cruising range of EVs, HESS should be charged repetitively [4][5].

WPT via magnetic resonance coupling (MRC) is suitable to charge EVs, due to its high transmission efficiency over large gaps [6][7]. For achieving maximum efficiency, load impedance control with a DC-DC converter was proposed [8]∼[10]. However, in this case, the charge power is fixed when the transmitter side voltage is constant. The charge power should also be considered because of the limited capacity of the HESS and its charge time design [11]∼[14]. The charge power control and transmission efficiency optimization should be performed on the receiver side to simplify the system.

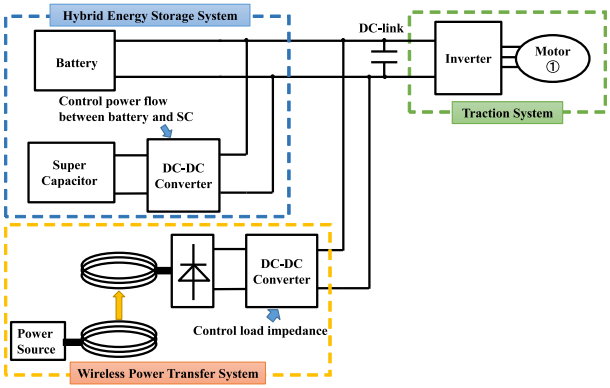

Fig. 1. Schematic of system which applies WPT to the HESS.

In this paper, a framework of HESS with WPT via magnetic resonant coupling is introduced for EVs application. The characteristics of WPT are explained, and it is shown that the load impedance for maximum efficiency is different from the load impedance for maximum power. Considering these characteristics, the charge power control by a DC-DC converter is proposed. The proposed method which applies feedforward controller is verified by experiments.

II. HESS with WPT charging system

Fig. 1 shows the schematic of system applied WPT to HESS considered in this work. This energy system can decrease the size of an energy storage system and optimize the energy system because the SC has a high power density and WPT can compensate for the low energy density of the HESS [15]. The charge power from WPT is absorbed by the battery and the SC or directly consumed by motors if motors are operating.

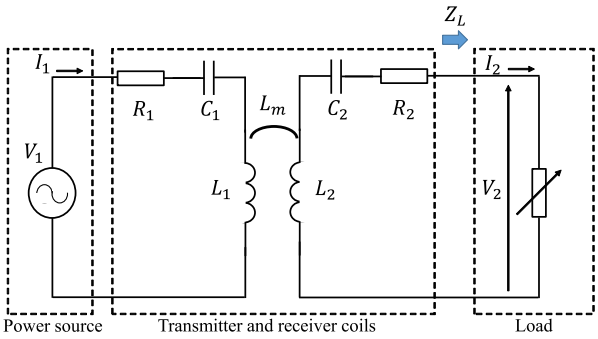

Fig. 2. Equivalent circuit of magnetic resonant coupling.

TABLE I
THE PARAMETERS OF COILS.

transmission side voltage:V_1	10V
Transmission frequency:f	100.9kHz
Inductance of transmitter coil : L_1	0.614mH
Inductance of receiver coil : L_2	0.616mH
Resistance of transmitter coil : R_1	1.5Ω
Resistance of receiver coil : R_2	1.5Ω
Capacitance of transmitter coil : C_1	4.05nF
Capacitance of receiver coil : C_2	4.04nF

The DC-link voltage is fixed to the battery voltage. The DC-DC converter connected to the SC is intended to control the current from the SC. In other words, this DC-DC converter controls power flow between the battery and the SC.

The DC-DC converter and rectifier connected to the receiver coil is applied to control the load impedance because the transmission efficiency and the charge power are decided by the mutual inductance and the load impedance. In other words, this DC-DC converter is applied to control the transmission efficiency and the charge power. In this paper, the charge power control from WPT by the DC-DC converter is proposed.

III. The Characteristics of WPT via Magnetic Resonant Coupling

The equivalent circuit of WPT via magnetic resonance coupling is illustrated in Fig. 2 [16]. L_1, L_2, C_1, C_2, R_1, and R_2 are decided by coils and do not have relation to the transmission distance or load condition. The mutual inductance L_m is related to transmission distance. Inductance and capacitance of the transmitter coil and the receiver coil satisfy

$$\omega_0 = \frac{1}{\sqrt{L_1 C_1}} = \frac{1}{\sqrt{L_2 C_2}}. \tag{1}$$

where ω_0 is the angular frequency of operation, because WPT via magnetic resonance coupling sends the power by electrical resonance.

V_1, I_1 are the effective values of transmitter side voltage and current. V_2, I_2 are the effective values of receiver side voltage and current. Z_L is the load impedance. The ratio of the effective value of the transmitter side voltage V_{10} and the receiver side voltage V_{20}, A_V are given as

$$A_V = \frac{V_{20}}{V_{10}} = j\frac{\omega_0 L_m Z_L}{R_1 Z_L + R_1 R_2 + (\omega_0 L_m)^2}. \tag{2}$$

The ratio of the effective value of the transmitter side current I_{10} and the receiver side voltage I_{20} A_I is given as

$$A_I = \frac{I_{20}}{I_{10}} = j\frac{\omega_0 L_m}{Z_L + R_2}. \tag{3}$$

The transmission efficiency A_P is given as

$$\eta = \frac{(\omega_0 L_m)^2 Z_L}{(Z_L + R_2)(R_1 Z_L + R_1 R_2 + (\omega_0 L_m)^2)} \tag{4}$$

and is equal to ratio of receiver to transmission power. The charge power P_L is given as

$$P_L = \frac{(\omega_0 L_m)^2 Z_L}{(R_1(R_2 + Z_L) + (\omega_0 L_m)^2)^2} V_{10}^2. \tag{5}$$

From Eq. (4), (5), η and P_L are decided by Z_L in the case of constant V_{10}. Fig. 4 shows η, P_L by the change of Z_L in the case when mutual inductance L_m is 38μH. The

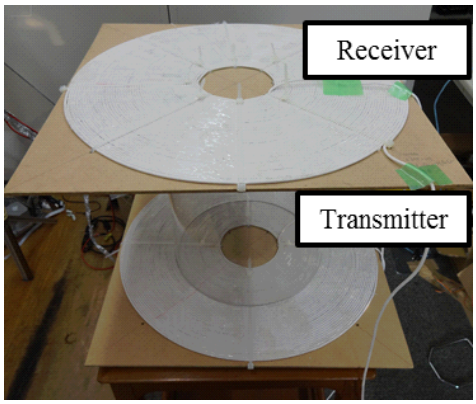

Fig. 3. Transmitter coil and receiver coil.

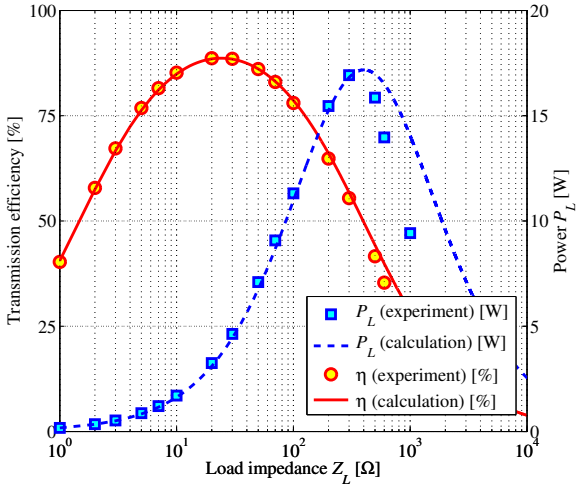

Fig. 4. Transmission efficiency and power in each load impedance.

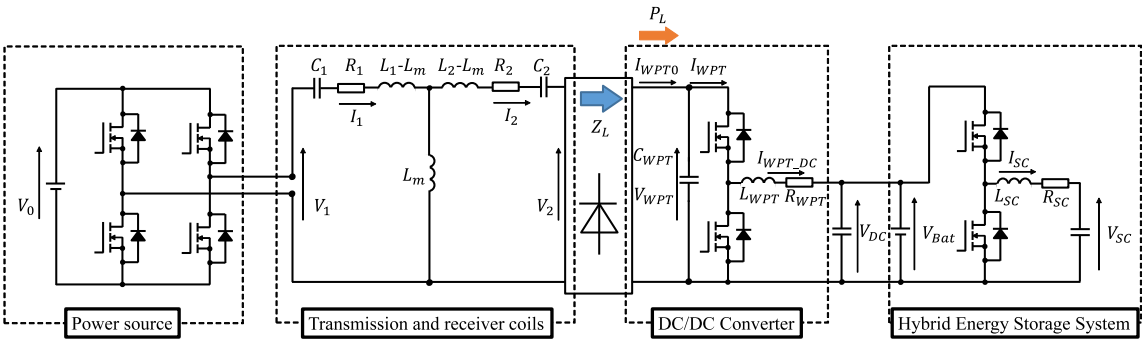

Fig. 5. The circuit of energy system.

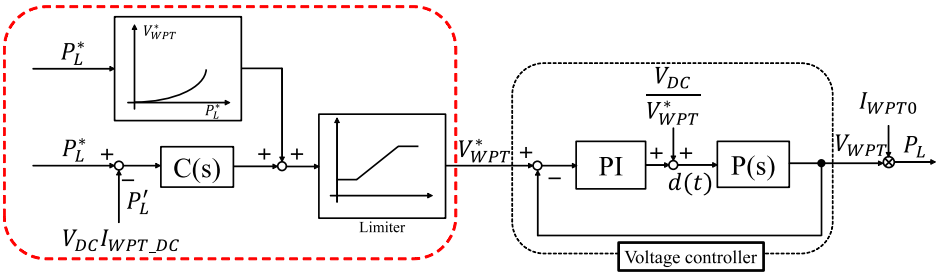

Fig. 6. The block diagram of the charge power control.

parameters of the coils are showed in TABLE. I. From these results, calculations and experiment results are almost the same. The load impedance Z_L which maximizes efficiency η and maximizes charge power P_L is different.

The load impedance which maximizes efficiency is given as

$$Z_{L\ \eta max} = \sqrt{R_2\left(\frac{(\omega_0 L_m)^2}{R_1} + R_2\right)} \tag{6}$$

derived from $\frac{\partial \eta}{\partial Z_L} = 0$.

In this case, the charge power is given as

$$P_{L\ \eta max} = \frac{(\omega_0 L_m)^2\sqrt{R_2\left(\frac{(\omega_0 L_m)^2}{R_1}+R_2\right)}V_{10}^2}{\left\{\sqrt{R_1R_2((\omega_0 L_m)^2+R_1R_2)}+R_1R_2+(\omega_0 L_m)^2\right\}^2}. \tag{7}$$

The load impedance which maximizes the charge power is given as

$$Z_{L\ PLmax} = \frac{(\omega_0 L_m)^2}{R_1} + R_2 \tag{8}$$

derived from $\frac{\partial P_L}{\partial Z_L} = 0$.

In this case, the maximum charge power is given as

$$P_{Lmax} = \frac{1}{4R_1\left(1+\frac{R_1R_2}{\omega_0 L_m}\right)}. \tag{9}$$

Assuming that the coil resistance is small enough, $Z_{L\ \eta max}$ is smaller than $Z_{L\ PLmax}$. In order to receive high power by high transmission efficiency, Z_L should be $Z_{L\ \eta max} < Z_L < Z_{L\ PLmax}$.

IV. The Charge Power Control Through Receiver Side Voltage Control

In this section, considering WPT characteristics, the control method of the charge power by DC-DC converter is explained. The equivalent circuit of WPT and, the HESS system is shown in Fig. 5. The block diagram of proposed charge power control is shown in Fig. 6. In this paper, two constraints are assumed:

- Voltage of the transmitter side is constant. Furthermore, voltage and frequency are known.
- The parameters of the coils are known.

A. Influence of square voltage source and rectifier

Fig. 7 shows the waveforms of V_1, V_2, I_1, and I_2. In Fig. 5, the power source operates as a square voltage source. Because the transmitter side current I_1 is a sinusoidal wave as shown in Fig. 7, only the fundamental wave of the transmitter side voltage V_1 affects the transmission. From its Fourier transform, the effective value of the fundamental wave V_{10} is shown as

$$V_{10} = \frac{2\sqrt{2}}{\pi}V_0. \tag{10}$$

It is well known that a WPT system has immittance characteristics [17]. The receiver side becomes a constant current source and V_2 becomes a square wave voltage by the rectifier like Fig. 7. Because the current of the receiver side is a sinusoidal wave, only the fundamental wave affects the

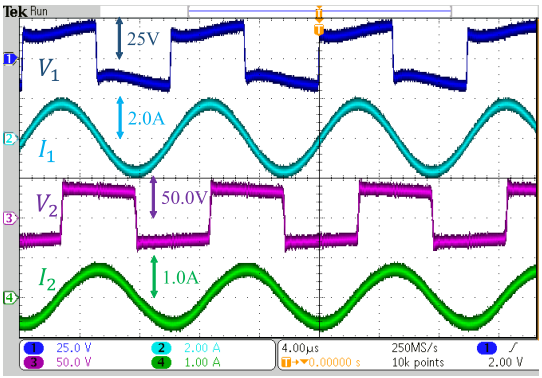

Fig. 7. The waveforms of V_1, V_2, I_1, and I_2

transmission. From its Fourier transform, the effective value of the fundamental wave V_{20} is given as

$$V_{20} = \frac{2\sqrt{2}}{\pi} V_{WPT}. \tag{11}$$

From Fig. 7, the power factors of the fundamental waves of the transmitter and receiver sides are 1. Therefore, the characteristics of WPT can be applied to the energy system in Fig.5.

B. Feedforward controller from the characteristics of WPT

From the characteristics of WPT, the load impedance Z_L can be derived to achieve the desired charge power P_L^*.

From Eq. (2), (5), The load impedance Z_L for achieving desired power is given as

$$Z_L = \frac{\alpha - \sqrt{\alpha^2 - 4R_1^2(R_1R_2 + (\omega_0 L_m)^2)^2 P_L^2}}{2R_1^2 P_L} \tag{12}$$

where α is defined as

$$\alpha = (\omega_0 L_m)^2 V_{10}^2 - 2R_1 P_L \left\{(\omega_0 L_m)^2 + R_1 R_2\right\}.$$

From Eq. (2), (12), in order to achieve desired power V_{20} is given as

$$V_{20} = \frac{\omega_0 L_m}{R_1} V_{10} - \frac{2P_L((\omega_0 L_m)^2 + R_1R_2)}{\omega_0 L_m V_{10} - \sqrt{(\omega_0 L_m V_{10})^2 - 4R_1 P_L((\omega_0 L_m)^2 + R_1R_2)}}. \tag{13}$$

The charge power can be controlled by the fundamental wave of receiver side voltage V_{20}. From Eq. (11)$\sim$(13), the voltage output of the DC-DC converter V_{WPT} in order to achieve the charge power P_L^* is calculated as

$$V_{WPT} = \frac{\omega_0 L_m}{R_1} V_0 - \frac{\pi^2}{4} \frac{((\omega_0 L_m)^2 + R_1R_2)P_L^*}{(\omega_0 L_m)V_0 - \sqrt{(\omega_0 L_m V_0)^2 - \frac{1}{2} R_1 P_L^* ((\omega_0 L_m)^2 + R_1R_2)}}. \tag{14}$$

This equation is applied as the feedforward controller for the charge power control. The mutual inductance L_m should be estimated because V_{WPT} is affected by L_m and it is not able to be measured directly. From Eq. (2), L_m can be estimated by measured variable values V_2, I_2 [18].

$$L_m = \frac{\frac{V_{10}}{I_2} + \sqrt{(\frac{V_{10}}{I_2})^2 - 4R_1(\frac{V_{20}}{I_2} + R_2)}}{2\omega_0} \tag{15}$$

In this paper, assuming that the mutual inductance L_m can be estimated accurately and known from the receiver side.

TABLE II
THE VERIFICATION OF THE RELATIONSHIP OF THE RECTIFIED VOLTAGE AND THE CHARGE POWER.

DC source voltage:E	15V
Battery voltage:V_{Bat}	12V
Inductance:L_{WPT}, L_{SC}	48mH
Condenser:C_{WPT}, C_{DC}	2500μF
Switching frequency	20kHz

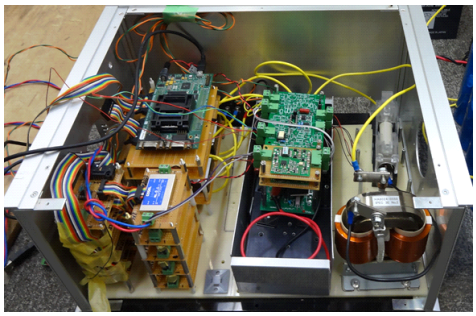

Fig. 8. The DC-DC converter for expriment.

C. Feedback controller to compensate the charge power error

In the actual system, the theoretical equation has error because the rectifier and the semiconductor switches have resistance. It is difficult to fix resonant frequency completely. As a result, only utilizing a feedforward controller is not enough to the achieve desired charge power. In order to compensate for the constant error of feedforward, a feedback controller is applied. The smoothed power $P_L' = V_{DC} I_{WPT\_DC}$ is used for the feedback controller because the frequency of the charge power is too high to be measured. The controller for feedback cannot be designed as a fast time constant controller because the dynamics of P_L and P_L' are different. However, in the case of charging to the energy storage system, the compensation of the constant error is the most important. The controller for the feedback loop can be designed as having more than ten times slower time constant than the voltage controller to compensate the constant error.

D. Limitation of rectified voltage from WPT characteristics

From Eq. (2), (6), and (8), values for V_{WPT} which maximize efficiency and power are showed respectively as

$$V_{WPT\ \eta max} = \sqrt{\frac{R_2}{R_1}} \frac{\omega_0 L_m}{\sqrt{R_1R_2} + \sqrt{R_1R_2 + (\omega_0 L_m)^2}} V_0 \tag{16}$$

$$V_{WPT\ Pmax} = \frac{\omega_0 L_m}{2R_1} V_0. \tag{17}$$

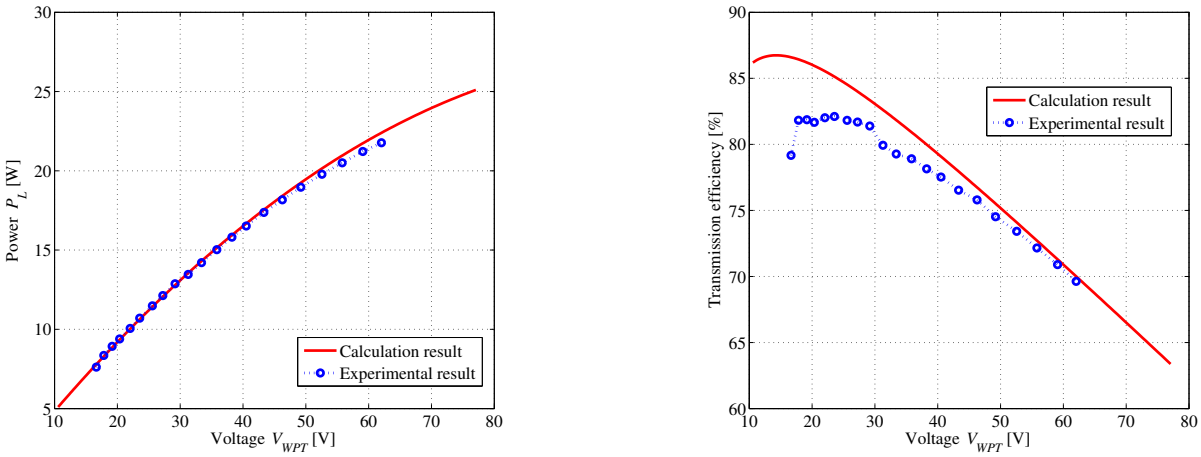

(a) The charge power (b) Transmission efficiency

Fig. 9. The relationship of the rectified voltage, the charge power, and transmission efficiency.

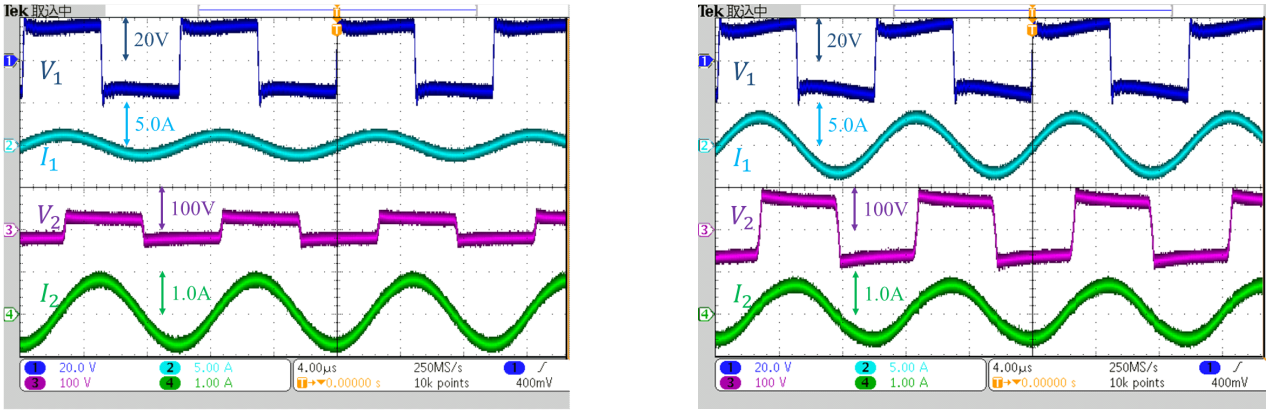

(a) V_{WPT} = 20V (b) V_{WPT} = 60V

Fig. 10. Experimental result of the waveforms.

From the characteristic of WPT, the rectified voltage V_{WPT} should be controlled in the region of Eq. (18).

$$V^*_{WPT} = \begin{cases} V_{WPT\ \eta max}(P^*_L \leq P_{L\ \eta max}) \\ V_{WPT}(P_{L\ \eta max} < P^*_L < P_{L\ PLmax}) \\ V_{WPT\ PLmax}(P^*_L \geq P_{L\ PLmax}). \end{cases} \quad (18)$$

V. Experimental Results and Analysis

A. The relationship of rectified voltage and the charge power

The parameters of the experiment are shown in TABLE. II. The experimental equipment is shown in Fig. 8.

Fig. 9 (a) shows the relationship of the rectified voltage and the charge power. Fig. 9 (b) shows the relationship of the rectified voltage and the transmission efficiency. From these results, the charge power and the transmission efficiency have a trade-off as seen in Fig. 4. From Fig. 9, the experimental results almost correspond to theoretical calculations. However, in the case of high receiver side voltage, the experimental results are different from the theoretical calculation. This error is caused by the parameter error of R_1 in particular because in the case of high receiver side voltage, the transmitter side current become high. Furthermore, the resonant frequency is not strictly matched and the voltage drop by the rectifier is not considered. The feedback controller can compensate this error.

Fig. 10 shows the waveforms of V_1, V_2, I_1, and I_2 in the case of V_{WPT} = 20V, 60V. From these results, when V_1 is constant, I_2 is almost constant. It means that WPT system indicates immittance characteristics [17].

B. The verification of the proposed power control

Fig. 11 shows the experimental results of the proposed power control without the feedback controller. From Fig. 11 (a), the voltage controller of the DC-DC converter operates well. From Fig. 11 (b), the average of the charge power P'_L is controlled to the reference P^*_L. P'_L has a delay because the voltage controller has a delay like Fig. 11. Furthermore, P'_L has an inverse response because the battery supplies small energy to C_{WPT} to control V_{WPT}. The constant error can be

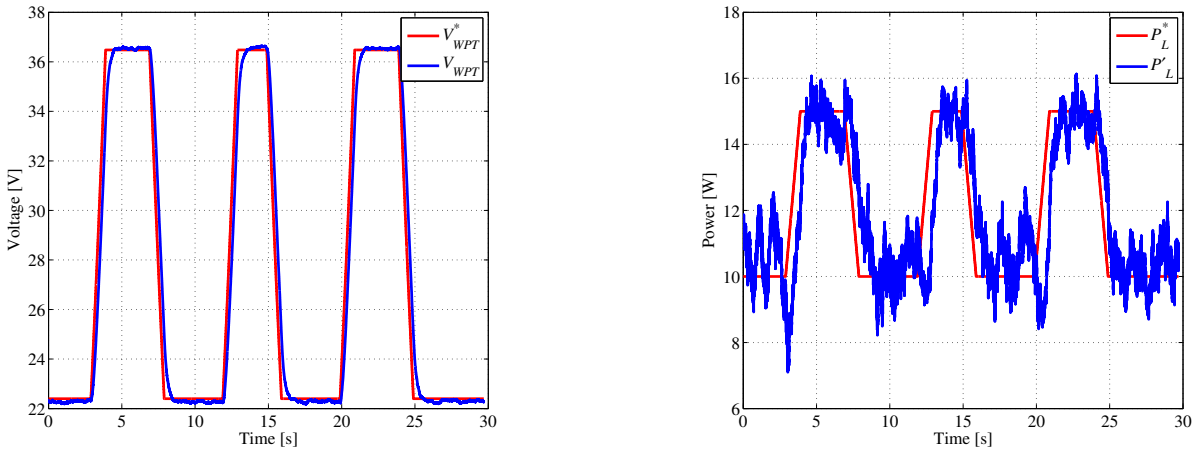

(a) The rectified voltage

(b) The charge power

Fig. 11. Experimental result of proposed control without feedback controller.

compensated by the feedback controller. From these results, the proposed controller can effectively control the charge power.

VI. Conclusion

In this paper, a framework of a HESS with a WPT charging system is proposed for application in EV . The characteristics of WPT are introduced and the charge power control through the receiver side voltage control is proposed because the transmitter side should be simple for EV applications. From the characteristics of WPT, the equation for controlling the charge power by a DC-DC converter is derived and is applied to a feedforward controller. Furthermore, the control method composed of feedback plus feedforward is proposed because there are differences from an ideal system in actual applications. The relationship of the rectified voltage and the charge power is verified by experiments and the feedforward controller of the proposed controller is verified by experiments. By the proposed controller, the charge power can be controlled on the receiver side. Future work is to verify the feedforward plus feedback controller by experiments and evaluate the controllability.

References

[1] J. Cao and A. Emadi, "A New Battery/UltraCapacitor Hybrid Energy Storage System for Electric, Hybrid, and Plug-In Hybrid Electric Vehicle," IEEE Transactions on Power Electronics, vol. 27, no. 1, pp. 122-132, Jan. 2012.

[2] B. Hredzak, V. G. Agelidis, and M. Jang, "A Model Predictive Control System for a Hybrid Battery-Ultracapacitor Power Source," IEEE Transactions on Power Electronics, vol. 29, no. 3, pp. 1469-1479, Mar, 2014.

[3] K. Kawashima, T. Uchida, and Y. Hori, "Development of a Novel Ultrcapacitor Electric Vehicle and Methods to Cope with Voltage Variation," in IEEE VPPC'09 Vehicle Power and Propulsion Conference, Sept, 2009.

[4] S. Ahn, N.P. Suh, and D.-H. Cho, "Charging up the road if electric vehicles could draw power from the streets, there's no telling how far they could go," IEEE Spectrum, vol. 50, pp.48-54 Apr, 2013.

[5] S. Li and C. C. Mi, "Wireless Power Transfer for Electric Vehicle Applications," IEEE Journal of Emerging and Selected Topics in Power Electronics, vol. PP, pp. 1, Apr. 2014.

[6] A. Kurs, A. Karalis, R. Moffatt, J. D. Joannopoulos, P. Fisher, and M. Soljacic, "Wireless Power Transfer via Strongly Coupled Magnetic Resonances," Science Express, vol. 317, no. 5834, pp.83-86 June, 2007.

[7] M. Kato, T. Imura, and Y. Hori, "New characteristics analysis considering transmission distance and load variation in wireless power transfer via magnetic resonant coupling," in IEEE INTELEC 34th International Telecommunications Energy Conference, Sept, 2012.

[8] M. Kato, T. Imura, and Y. Hori, "Study on Maximize Efficiency by Secondary Side Control Using DC-DC Converter in Wireless Power Transfer via Magnetic Resonant Coupling," in IEEE EVS27 International Battery, Hybrid and Fuel Cell Electric Vehicle Symposium, Nov, 2013.

[9] K. Takuzaki and N. Hoshi, "Consideration of Operating of Secondary-side Converter of Inductive Power Transfer System for Obtaining High Resonant Circuit Efficiency," IEEJ Transactions on Industry Applications, vol. 32, no. 10, pp. 966-975, Apr, 2012.

[10] M. Fu, C. Ma, and X. Zhu, "A Cascaded Boost-Buck Converter for High Efficiency Wireless Power Transfer Systems," IEEE Transactions on Industrial Informatics, vol. PP, pp. 1, Nov, 2013.

[11] H. L. Li, A.P. Hu, G. A. Covic, and C. S. Tang, "A New Primary Power Regulation for Contactless Power Transfer," in IEEE international conference on Industrial Technology 2009, pp. 1-5 Feb, 2009.

[12] W. Chwei-Sen, O. H. Stielau, and G. A. Covic, "Design considerations for a contactless electric vehicle battery charger," IEEE Transactions on Industrial Electronics, vol. 52, pp. 1308-1314, Oct, 2005.

[13] J. U. W. Hsu, A.P. Hu, and A. Swain, "A wireless Power Pickup Based on Directional Tuning Control of Magnetic Amplifier," IEEE Transactions on Industrial Electronics, vol. 56, pp. 2771-2781, July, 2009.

[14] W. Zhong and S. Y. R Hui, "Maximum Energy Efficiency Tracking for Wireless Power Transfer Systems," IEEE Transactions on Power Electronics, vol. PP, 2014 (early access)

[15] T. Hiramatsu, X. Huang, and Y. Hori, "Capacity Design of Supercapacitor Battery Hybrid Energy Storage System with Repetitive Charging via Wireless Power Transfer," in IEEE PEMC2015 16th International power Electronics and Motion Control Conference, pp578-583, Sep, 2014.

[16] T. Imura, H. Okabe, T. Uchida, and Y. Hori, "Study on Magnetic and Electric Coupling for Contactless Power Transfer Using Equivalent Circuits," IEEJ Transactions on Industry Applications, vol. 130, no. 1, pp. 83-92, Aug, 2010 (in Japanese).

[17] H. Irie and Y. Tahara, "Cascade Configuration of T-LCL-Type and T-CLC-Type Immittance Converters in Non-Contact Energy Transfer Systems," IEEJ Transactions on Industry Applications, vol. 129 no. 5 pp. 511-517 2009 (in Japanese).

[18] V. Jiwariyavej, T. Imura, and Y. Hori, "Coupling Coefficients Estimation of Wireless Power Transfer System via Magnetic Resonance Coupling using Information from Either Side of the System," in Proc. the 2012 International Conference on Broadband and Biomedical Communication, Nov 2012.